sustainability

MDPI

Article

Power Management and Control of a Hybrid Electric Vehicle Based on Photovoltaic, Fuel Cells, and Battery Energy Sources

Naoui Mohamed [1], Flah Aymen [1], Abdullah Altamimi [2,*], Zafar A. Khan [3,4] and Sbita Lassaad [1]

1 Processes, Energy, Environment and Electrical Systems (Code: LR18ES34), National Engineering School of Gabès, University of Gabès, Gabès 6072, Tunisia; mednaouiing@yahoo.com (N.M.); aymen.flah@enig.u-gabes.tn (F.A.); sbita.lassaad@yahoo.fr (S.L.)
2 Department of Electrical Engineering, College of Engineering, Majmaah University, Al-Majmaah 11952, Saudi Arabia
3 Electrical Engineering Department, Mirpur University of Science and Technology, Mirpur 10250, Pakistan; zafarakhan@ieee.org
4 School of Computing and Engineering, Institute for Innovation in Sustainable Engineering, University of Derby, Derby DE22 1GB, UK
* Correspondence: a.altmimi@mu.edu.sa

Abstract: This paper deals with an energy management problem to ensure the best performance of the recharging tools used in electric vehicles. The main objective of this work is to find the optimal condition for controlling a hybrid recharging system by regrouping the photovoltaic cells and fuel cells. The photovoltaic and fuel cell systems were connected in parallel via two converters to feed either a lithium battery bank or the main traction motor. This combination of energy sources resulted in a hybrid recharging system. The mathematical model of the overall recharging system and the designed power management loop was developed, taking into account multiple aspects, including vehicle loading, the stepwise mathematical modelling of each component, and a detailed discussion of the required electronic equipment. Finally, a simplistic management loop was designed and implemented. Multiple case studies were simulated, statistical approaches were used to quantify the contribution of each recharging method, and the benefits of the combination of the two sources were evaluated. The energetic performance of an electric vehicle with the proposed hybrid recharging tool under various conditions, including static and dynamic modes, was simulated using the MATLAB/Simulink tool. The results suggest that despite the additional weight of PV panels, the combination of the PV and FC systems improves the vehicle's energetic performance and provides a higher charging capacity instead of using an FC alone. A comparison with similar studies revealed that the proposed model has a higher efficiency. Finally, the benefits and drawbacks of each solution are discussed to emphasise the significance of the hybrid recharging system.

Keywords: battery; fuel cells; gas emissions; hybrid power system; photovoltaic; power management

Citation: Mohamed, N.; Aymen, F.; Altamimi, A.; Khan, Z.A.; Lassaad, S. Power Management and Control of a Hybrid Electric Vehicle Based on Photovoltaic, Fuel Cells, and Battery Energy Sources. *Sustainability* **2022**, *14*, 2551. https://doi.org/10.3390/su14052551

Academic Editors: Attia El-Fergany, Mahmoud El-kholy and Mohamed El-Hameed

Received: 8 December 2021
Accepted: 16 February 2022
Published: 23 February 2022

1. Introduction

The efficiency of the hybrid electric vehicle (HEV) powertrain depends entirely on the performance of the driving behaviour and the devices used, such as converters, switches, and motor drives [1]. Apart from the HEV physical components, significant improvements are being made in HEV software to improve the efficiency of the systems [2].

Generally, an HEV consists of an internal combustion engine (ICE) and a motor for propulsion. Vehicle manufacturers are focusing on HEVs because environmental safety has become a global concern. Hydrogen was introduced as a fuel source for vehicles to keep the atmosphere clean. Fuel cells (FCs) have been considered as a possible solution to replace traditional gasoline vehicles (GVs) [3–6]. This is due to limited emissions, less reliance on crude oil, and the heightened fuel economy, which could significantly improve air quality, energy stability, and climate change. Based on the advantages of FC systems and the benefits of renewable energy systems, integrating photovoltaic cells into electric vehicles can potentially increase their available energy, even if they are on the road [5,7].

Many modelling studies focusing on the transient power characteristics of FC systems have been conducted, such as [8,9]. In addition, much research has focused on the fuel-cycle analysis of emissions and the energy consumption of transportation fuels, as found in [10]. However, few studies have examined the efficiency of fuel cell systems in relation to fuel-cycle emissions and energy consumption [11]. Some studies have analysed hybrid FC and PV systems, such as [12,13], which aimed to find a simple and efficient control topology.

This study proposes a new multi-source system for EVs that comprises an FC system, a PV system, and a battery system. It tests and validates whether the integration of PV cells with the FC solution will be advantageous to solve the constraints of the existing literature. A hybrid energy source is created for HEVs by combining FC and PV systems, which can be used to recharge a vehicle. This study aims to optimise the efficiency for improving vehicle autonomy by coupling these energy sources. Therefore, a power management control loop was designed to control these two energy sources to help charge vehicles in three different cases. The results of this study indicate a difference when using a combination of energy sources and proves that integrating PV cells is profitable, even if additional weight is introduced [14,15].

Thus, the energy efficiency of the hybrid recharging tool was tested under various simulation conditions. The importance of this hybrid system was validated by monitoring the battery's state of charge (SOC) while the vehicle was accelerating under different values, and the energetic performance was compared. This analysis also produced statistical results that classified and organised the proposed recharging solutions according to vehicle speed and then found the best conditions for each studied recharging solution. Thus, this paper presents an approach to managing the hybrid energy source in an EV to optimise the battery charging system. The proposed power management flowchart manages two energy sources [2] based on predefined rules and is fixed according to the vehicle speed and battery state of charge [16].

The rest of this paper is organised as follows. After a general introduction, the electric vehicle model is described, and its internal components are presented in Section 2. Then, in Section 3, the hybrid recharging tool is described by showing the necessary PV and FC mathematical equations. Section 4 shows the related results, which study the energetic performance of the hybrid recharging tool. This is carried out after showing the energy management block and describing its running mode. Many results are shown in this section, and a critical discussion is applied for each simulation step. Finally, Section 6 is intended for resuming this work and presents future endeavours.

2. Electric Vehicle Description

2.1. General Review

An EV is composed of two models, the hybrid version and the pure EV. Figure 1 shows the two different architectures of the pure electric vehicle model and the hybrid version. The only difference between the two models is the internal combustion engine (ICE) present in the hybrid model. The initial pack of components regroups an energy source alongside the battery system. This block is connected to an electronic power converter to feed the main electric motor. The function block needs a control system in addition to a calculator with a high-speed processor to supervise all the processes of energy management and vehicle speed control [17,18].

Many problems and advantageous descriptions can be found for each of these models in [19]. Considering the problems of the environment and gas emissions, it is easy to conclude that the pure electric vehicle field has encouraged researchers to make this transport solution more efficient. Optimising a motor's size and improving the battery technologies by making various recharging solutions are the different fields in this research sector [20–22].

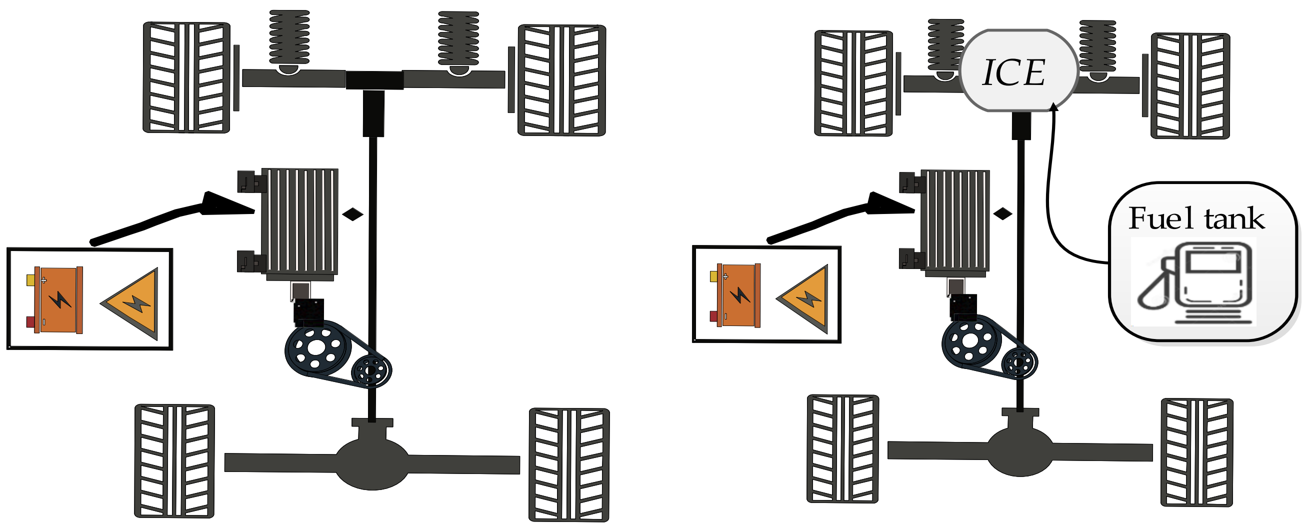

(**a**) (**b**)

Figure 1. Two electric vehicles models: (**a**) battery electric vehicle; (**b**) hybrid electric vehicle.

2.2. The Associated Converters in the Electric Vehicle Model

The composition of the EV systems and, particularly, the energy sources determine the energy transferred through the battery charger. The challenges of designing an HEV involve particular compositions, including a PV system, a battery system, the mechanical gear model, the fuel cell generator, the associated converters, and the main electric motor [23].

This study intends to propose a new multi-source system for EVs that comprises an FC system, PV system, and battery system. A conceptual depiction of the proposed system is given in Figure 2. The system consists of a DC/DC converter, buck-boost converter, and DC/AC converter. The DC/DC converter adjusts the electric current to charge the battery. Generally, the charging topology of electric vehicle applications comprises front-end (AC-DC) and back-end (DC-DC) converters. In the first stage of AC-DC converter topology, the power factor correction (PFC) is adjusted while the DC-DC converter topology controls the voltage level to make it appropriate for EV battery charging. Mainly, there are multiple DC-DC converters for different applications, and the desired output power level decides the converter type selection [24]. Some challenging factors, such as safety, efficiency, cost, switching frequency, and power density, need to be considered while designing a DC-DC converter for a battery charger for EVs. The DC-DC converters in EV charging applications can be divided into unidirectional and bidirectional based on charging systems [24]. The authors in [24,25] discussed several unidirectional and bidirectional DC-DC converter topologies based on EVs charging systems. The advantages of bidirectional over unidirectional converters, along with their challenging issues, are examined in detail in [26]. For a bidirectional elevator chopper topology, a double active switch is needed, while an inductor in the output is not essential, making it less costly and easy to implement. There are some DC-DC converters, such as a multi-stage integrated charging solution for EVs, which are more efficient than the one used, but the cost of the converter is very high [24,26]. Therefore, bidirectional non-isolated DC-DC converters, including conventional DC-DC converters, are common, with a low cost, high reliability, fast control, and a wide voltage range in two operating conditions [27]. These topologies are popularly used with continuous power supplies and hybrid electric cars, as they provide a high efficiency due to their high static voltage gains and low voltage stress in both boost and buck mode [24,27].

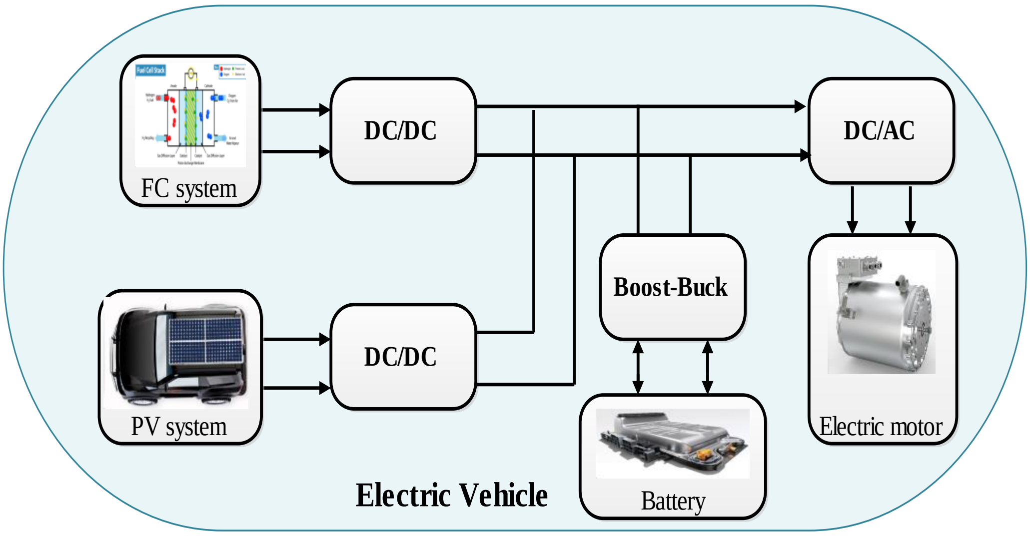

Figure 2. Multi-source system for an electric vehicle.

In this application, a single source or both energy sources can be used to charge the battery. The buck-boost converter is responsible for the charging or the discharging state of the battery. The charging or the discharging state depends on the electric motor's energetic needs. When the electric motor is in the traction phase, the surplus energy from the PV and the FC sources can be used to charge the battery, whereas, in the discharging state, the battery can provide the low power to operate the motor. Three possible cases can be observed, i.e., a recharge using only the PV system, a recharge using only the FC system, or the hybrid recharge using two energy sources.

3. The main Components of the Electric Vehicle

3.1. Lithium-Ion Battery Model

Numerous battery models can be found in the existing literature, as indicated in these studies [28,29]. The lithium model can provide optimum performance, and its detailed function is given in Figure 3 [30–32].

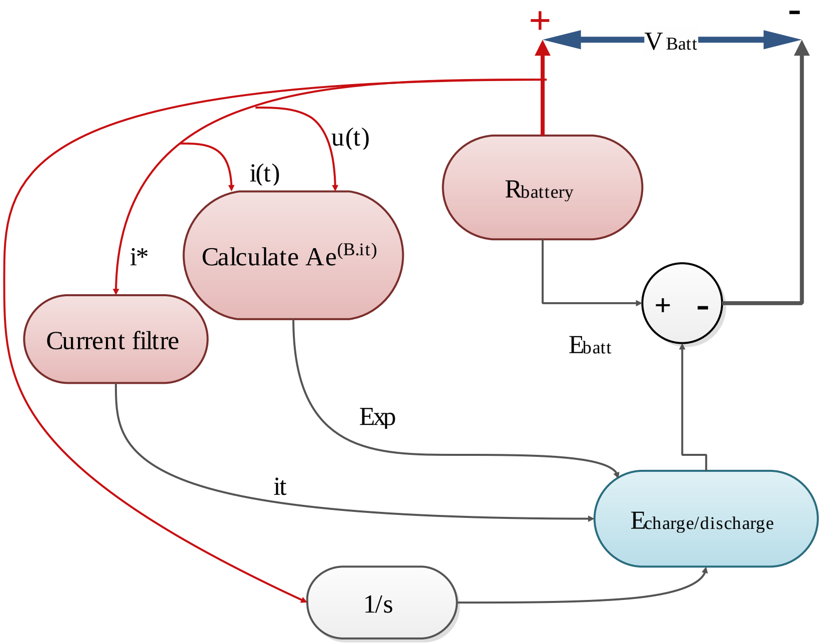

Figure 3. Electrical diagram of a lithium-ion battery.

The battery voltage model, noted by $E_{charge/discharge}$ [31,33], can be defined in Equation (1), and this equation is also used to calculate the nonlinear voltage E_{batt}.

$$\begin{cases} E_{charge} = E_0 - K\frac{Q}{Q-it} \times it - K \times \frac{Q}{Q-it} \times i^* + A \times e^{(-B \cdot it)} \\ E_{discharge} = E_0 - K\frac{Q}{Q-it} \times it - K \times \frac{Q}{0.1\,Q+it} \times i^* + A \times e^{(-B \cdot it)} \end{cases} \quad (1)$$

The state of charge can be calculated using Equation (2):

$$\begin{cases} SOC = \frac{Q(t)}{Q_{Max}} \times 100 \\ Q(t) = Q(0) - \int_0^t \eta_b I_b dt \end{cases} \quad (2)$$

where I_b = battery current and η_b = battery performance [34].

These two equations were used inside a battery power model to generate the equivalent battery power noted by P_{batt}. The details of this mathematical model can be found in [35].

3.2. Electronic Equipment for The Recharging Solution

3.2.1. Bidirectional Converter

The electrical system of an electric vehicle depends mainly on a group of converters. The buck-boost converter, based on semiconductors, is the most important element inside this loop. Wide band-gap semiconductors, such as SiC, GaN, and diamond, are needed for megawatt power applications. Such applications require highly efficient, lightweight, high-density power converters operating at high temperatures. The specific properties of various semiconductors are listed in Table 1 [36–38].

Table 1. Semiconductor properties.

	Si	4H-SiC	6H-SiC	GaAs	GaN	Diamond
Energy band-gap, E_g (eV)	1.12	3.03	3.26	1.43	3.45	5.45
Critical electric field, E_c (MV/cm)	0.25	2.2	2.5	0.4	2	10
Saturated electron drift velocity, V_{sat} (cm/s)	1×10^7	2×10^7	2×10^7	1×10^7	2.2×10^7	2.7×10^7
Thermal conductivity I (W/cm-K)	1.5	4.9	4.9	0.46	1.3	22
Electron mobility, μ_n (cm^2/s)	1350	1000	500	8500	1250	2200
Dielectric constant, e_t	11.9	10.1	9.66	13.1	9	5.5

The key energy source is the battery, which is connected to an electric motor through a two-quadrant DC-DC converter. The converter has two functions, i.e., a voltage minimisation step and a voltage elevation phase. In addition, they are assured by a buck-boost DC converter. These operation functions are required, as the storage system has positive and negative signs, allowing bidirectional energy transfer [39].

The bidirectional DC-DC converter operates in boost mode when the IGBTs related to the switch "S1" and the diode "D2" are closed, and it is in conduction status. Therefore, the battery is in discharging mode, and the current of the inductor, i_L, has a positive sign. By merging the equation of the mesh law, the mathematical model of the DC-DC converter, which operates in boost mode, is given by the differential system as in Equation (3):

$$\begin{cases} \frac{di_L}{dt} = -\frac{(1-u_1)}{L} V_{dc} + \frac{V_{bat}}{L} - \frac{R}{L} i_L \\ i_{bat} = (1-u_1) i_L \end{cases} \quad (3)$$

The bidirectional DC-DC converter operates in buck mode when the IGBTs related to the switch S2 and the diode D1 are closed so that they can conduct. Then, in this case, the battery is in charging mode and the current of the inductor, i_L, has a negative sign. The mathematical model of the DC-DC converter is in buck mode and is given the same form of Equation (3) and by considering $u_2 = (1 - u_1)$, which represents the control signal of the second IGBT.

3.2.2. Converter Losses

The power losses of the MOSFET or the IGBT in the switching or the conduction phases, the corresponding power losses of the diode in the conduction phase, and the inductor and capacitor equivalent power losses in the DC-DC boost and buck-boost converters are evaluated in this section. The following formulas that can be used to compute the equivalent losses in these components were obtained from [40] and summarised as follows:

MOSFET Losses

The drain-source on-resistance ($R_{DS\ (on)}$) causes conduction loss in MOSFETs. Changes in the drain current and junction temperature affect the on-resistance. The voltage drop is calculated by Equation (4) [40]:

$$V_{DS}(i_d, T) = i_D \times R_{DS(on)}(i_D, T) \tag{4}$$

Equation (5) can be used to express the instantaneous value of the conduction loss:

$$P_{con,M}(t) = V_{DS}(t) \times i_D(t) = i_D(t)^2 \times R_{DS(on)} \tag{5}$$

The MOSFET switching loss is primarily determined by the on and off state energy losses. The MOSFET switching loss is computed by taking into account the loss associated with the MOSFET's on and off states. The on-state energy loss is determined without taking into account the loss associated with MOSFET reverse recovery. However, the loss associated with the anti-parallel diode's reverse recovery process is taken into account when computing the on-state loss. The switching loss of a MOSFET is calculated as in Equation (6):

$$P_{sw,M} = \left(E_{on,M} + E_{off,M}\right) f_{sw} \tag{6}$$

The MOSFET datasheets include the values for the parameters utilised in the theoretical computation of conduction and switching losses.

IGBT Losses

The conduction and switching losses of IGBTs are estimated in the same way that MOSFET conduction and switching losses are calculated. The MOSFET drain, source, and gate are analogous to the IGBT collector, emitter, and base, respectively. The conduction loss in an IGBT is calculated as follows:

Equation (7) gives the immediate value of the conduction loss associated with IGBT:

$$P_{con,IGBT}(t) = V_{CE}(t) \times i_C(t) = (V_{CEO} + R_C i_C(t)) i_C(t) = V_{CEO} i_C(t) + R_c i_c\ (t)^2 \tag{7}$$

Equation (8) is the average value of the IGBT conduction loss:

$$P_{con,IGBT} = \frac{1}{T_{sw}} \int_0^{T_{sw}} V_{CE}(t) \times i_C(t) dt = \frac{1}{T_{sw}} \int_0^{T_{sw}} (V_{CEO} + R_C i_C) i_C(t) dt = V_{CEO} I_{Cav} + R_c i_{Crms}^2 \tag{8}$$

In this phase, the IGBT switching loss is given by Equation (9):

$$P_{sw,IGBT} = \left(E_{on,IGBT} + E_{off,IGBT}\right) f_{sw} \tag{9}$$

The IGBT datasheet provided the values for the parameters needed in the theoretical calculation of the conduction and switching losses.

Diode Losses

There are two types of losses in a boost converter diode: conduction and switching losses. The conduction loss and the switching loss in diode can be expressed in Equations (10) and (11):

$$P_{con,D} = V_{fD} \times I_0 \tag{10}$$

$$P_{sw,D} = Q_c \times V_0 \times f_{sw} \tag{11}$$

Inductor Losses

The inductor has significant losses, such as conduction and copper losses. Equation (12) is a breakdown of these losses:

$$P_L = I_{Lrms}^2 \ R_{dc} \tag{12}$$

$$where\ ,I_{Lrms}^2 = I_0^2 + \frac{\Delta I^2}{12} \tag{13}$$

where ΔI is the ripple current and ΔI^2 can be neglected.

Therefore, the inductor conduction loss can be simplified by:

$$P_L = I_0^2 \times \ R_{dc} \tag{14}$$

Capacitor Losses

The losses in the capacitor can be stated as:

$$P_c = I_c^2 \times \ ESR \tag{15}$$

4. Modelling of the Hybrid Recharging Tool

4.1. The First Recharging Tool: The Photovoltaic Generator

The PV system consists of many solar cells. They are the essential electrical component used to convert solar irradiation into electricity and can be used in different applications, including electric vehicles. Many studies have proposed numerous models for the solar cell, as in [41]. Figure 4 shows a commonly used electrical model of a solar cell [42,43].

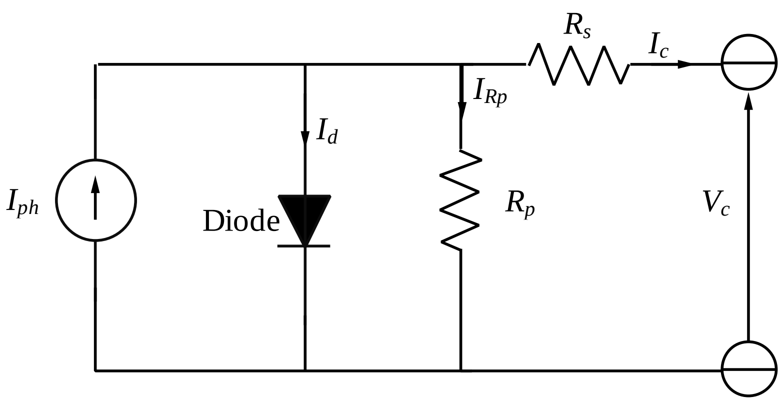

Figure 4. Equivalent solar cell's electric circuit.

The current, I_c, can be given by Equation (16):

$$I_c = I_{ph} + I_{sh} + I_d \tag{16}$$

where I_c is the cell current, I_{ph} is the photocurrent generated by the current source, I_d is the current shunted through the intrinsic diode, and I_{sh} is the current delivered by the parallel resistance.

The current I_{ph} (PV cell current) can be evaluated by Equation (17):

$$\begin{cases} I_{ph} = \frac{G}{G_{ref}}\left(I_{rs-ref} + \left[K_{SCT}\left(T_c - T_{c-ref}\right)\right]\right) \\ I_d = I_{rs}\left(e^{\frac{q(V_c+R_sI_c)}{\alpha kT}} - 1\right) \\ I_{sh} = \frac{1}{R_p}(V_c + R_sI_c) \end{cases} \quad (17)$$

The *PV* generator model depends on the connection types (parallel or series), and the number of solar cells, N_p and N_s, respectively, as shown in Figure 5 and explained in Equation (18).

$$\begin{cases} I_P = N_P I_C \\ V_P = N_S V_C \end{cases} \quad (18)$$

Figure 5. PV cells placed on a vehicle.

The resistances R_s are considered very small compared to R_p, and based on this supposition, the model uses $R_p = \infty$ and $R_s = 0$. So, the current, I_p, can be given by Equation (19).

$$I_p = N_p I_{ph} - \left[N_p I_{rs}\left(e^{\left(\frac{q(V_p)}{n\beta n_S T_C N_S}\right)-1}\right)\right] \quad (19)$$

The equivalent given power from this renewable energy generator can be presented in [44], and the parameter used for calculating this energy is noted as P_{PV}.

4.2. The Second Recharging Tool: Fuel Cell Model

The fuel cell proton exchange membrane [12] uses air and hydrogen as the fuel sources [45,46]. Equation (20) gives the rates of conversion (utilisations) of hydrogen (X_{fH2}) and oxygen (X_{fO2}), which are determined in block A as follows:

$$\begin{cases} X_{f_{O_2}} = \frac{n^r_{o_2}}{n^{in}_{o_2}} = \frac{60{,}000 \times R \times T \times i_{fc}}{2 \times z \times F \times P_{air} \times V_{air} \times y\%} \\ X_{f_{H_2}} = \frac{n^r_{H_2}}{n^{in}_{H_2}} = \frac{60{,}000 \times R \times T \times i_{fc}}{z \times F \times P_{fuel} \times V_{fuel} \times x\%} \end{cases} \quad (20)$$

The partial pressures and the Nernst voltage (E_n) are determined in block B and are shown in Equations (21) and (22) [12,47]:

$$\begin{cases} P_{H_2} = \left(1 - U_{fH_2}\right) x\% P_{fuel} \\ P_{H_2o} = \left(\omega_{fc} + 2y\% U_{fO_2}\right) P_{air} \\ P_{O_2} = \left(1 - U_{fO_2}\right) y\% P_{air} \end{cases} \quad (21)$$

$$\begin{cases} E_n = 1.229 + (T - 298) \times \frac{-44.43}{zF} + \frac{RT}{zF} \ln\left(P_{H_2} \times P_{O_2}^{\frac{1}{2}}\right) & when\ T \leq 100\ ^\circ\mathrm{C} \\ E_n = 1.229 + (T - 298) \times \frac{-44.43}{zF} + \frac{RT}{zF} \ln\left(\frac{P_{H_2} \times P_{O_2}^{\frac{1}{2}}}{P_{H_2O}}\right) & when\ T > 100\ ^\circ\mathrm{C} \end{cases} \quad (22)$$

where P_{H2O} represents the partial pressure of water vapour inside the stack (atm) and w represents the oxidant percentage of water vapour (%).

Then, the exchange current (i_0) and the open-circuit voltage (E_{oc}) can be computed based on the Nernst voltage (E_n) and the partial pressures of gases, as in Equations (23) and (24) [12]:

$$E_{oc} = K_c E_n \quad (23)$$

$$i_0 = \frac{zFk\left(P_{H_2} + P_{O_2}\right)}{Rh} e^{-\left(\frac{\Delta G}{RT}\right)} \quad (24)$$

Based on the previously cited reference [12], at nominal operating conditions, the study uses the polarisation curve while some additional parameters are taken into account. These parameters include the stack efficiency, composition of fuel and air, supply pressures, and ambient temperatures. The nominal rates of gas conversions can be computed as in Equation (25).

$$\begin{cases} X_{fH_2} = \frac{\eta_{nom} \Delta h^0_{(H_2O)g} N}{zFV_{nom}} \\ X_{fO_2} = \frac{60{,}000 \times R \times T_{nom} \times N \times I_{nom}}{2 \times z \times F \times P_{airnom} \times V_{Ipm(air)nom} \times 0.21} \end{cases} \quad (25)$$

All of these equations were used to estimate the given fuel cell power, noted $P_{FC,}$ and the corresponding mathematical model of this output can be found in [48].

5. Results and Discussion

5.1. Simulation Conditions

The EV model was simulated using the MATLAB/Simulink tools. The proposed model was validated under different conditions related to the vehicle status and the hybrid system parameters. Therefore, this section presents and discusses the obtained results using the proposed models. It concentrates on the control and power management efficiency concerning electric vehicle speed. The vehicle parameters and the motor and battery pack specification used in simulations are listed in Tables 2 and 3 [28,41]. Figure 6 shows the explanatory diagram of the overall system; this figure correlates the mathematical model with the proposed model.

Table 2. Parameters of the vehicle.

Parameters	Symbol	Values
Vehicle mass	m	1800 kg
Rolling resistance	f_r	0.01
Air density	ρ_{air}	1.2 kg $\times$ m^2
The frontal surface area of the EV	A_f	2.6 m^2
Tire radius	R	0.32 m
Aerodynamic drag coefficient	C_d	0.41

Table 3. Parameters of the electric motor and battery pack.

Parameters	Symbol	Values
Shaft power	P_u	50 kW
Pole pairs	P_p	2
Resistance of stator	R_s	2.63 Ω
Resistance of rotor	R_r	2.42 Ω
Mutual inductance	M	0.253 H
Rotor and stator self-inductance	$L_s = L_r$	0.214 H
Inertia moment	J	0.03 kg m^2
Viscous friction	f	0.0002 N m × s^2
	Battery parameters	
Battery voltage	V_{bat}	72 V
Rated Capacity	Q	68 Ah
Rated Power	P_{bat}	50 kW
Type	*Lithium battery*	-

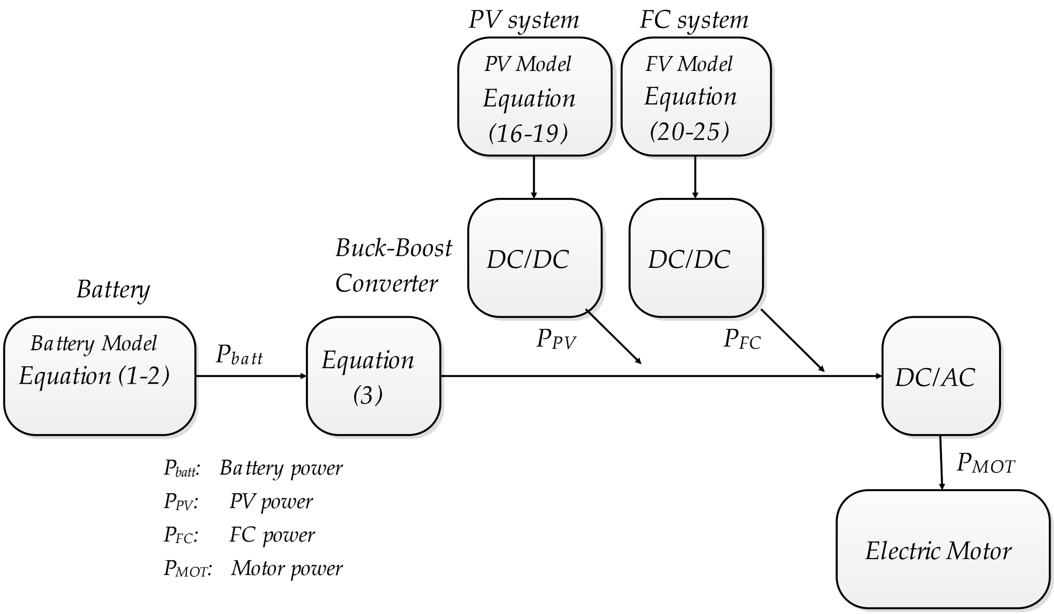

Figure 6. Diagram of the global system.

Given the high costs of a lithium battery, minimising the total energy consumed is important. A more complex control strategy is needed because, in this case, the energy stored is small. It is important to detect any variables that need to be sensed, such as instant battery voltage, battery charge state, instant battery current, initial conditions of the battery, battery capacitor current, etc. The vehicle's speed must also be taken into account, as all the energy is required when the vehicle is going to start. On the other hand, when the vehicle is operating at high speeds, the fuel cell needs to give important energy to recover the electric motor's consumption. To test the hybrid system's efficiency, a driving route, as presented in Figure 7a was chosen. Figure 7b gives the corresponding vehicle speed for the given acceleration form as it is in Figure 7a.

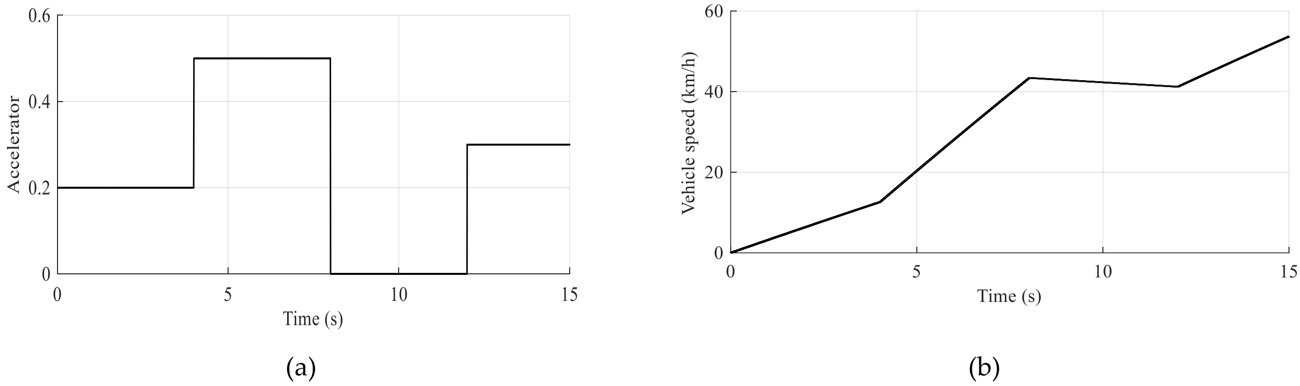

Figure 7. Vehicle speed: (**a**) accelerator; (**b**) speed.

5.2. Power Management and Control

The electric vehicle (EV) with storage batteries must be recharged daily. A hydrogen supply is required for those using FCs to supply electrical energy. It is only during the sunshine cycle that solar energy provides energy for those fitted with PV systems. The electric vehicle uses batteries for storage, but fuel cell or hydrogen vehicles, solar electric vehicles, or a combination of solar, FC, and battery can be a competitive option due to less autonomy. Coordination between the various energy sources includes control of power management. Several researchers have worked on the energy management system, and each study was used according to the application. For example, in [49–51], the authors used fuzzy logic in the ICE, battery application, and optimisation-based energy management strategy. In [52], the authors studied the topologies and integrated energy management strategies to improve system power loss efficiency. Most of the research only used two energy sources in their control algorithm, making the control topology more complex if a third source was used; that is because updating the fuzzy rules or updating a neural network controller needs a significant change and an extensive database. In this study, the presented control topology seems more straightforward than when even three energy sources were used, as the control tool is based on relays [53].

Based on these studies, the battery bank device was chosen in our work to begin generating electricity. The fuel cell uses hydrogen to generate electricity, and the photovoltaic system at least works to adapt solar irradiation to electrical energy supplied to a DC bus. The total power is measured as explained in [54] and in Equation (26), and Figure 8 shows a proposed diagram of the hybrid energy storage system and power management for EV [55].

$$P_{Motor} = P_{PV} + P_{FC} + P_{batt} \tag{26}$$

When the EV is under partial shading, such as in a garage, parking lot, or any other type of shelter, the solar radiation's power will be at its lowest (zero). The battery will drive the car, and the FC will participate when the acceleration demand increases. The obtained results of the power evolution for the previously cited simulation conditions are shown in Figure 9, which confirms Equation (26) and proves the mathematical models and their description. Figure 9a shows the PV system power for the various acceleration forms, as shown in Figure 7a. Based on new photovoltaic cell technologies [56,57], the PV can generate 9W as its maximum energy for the best irradiation factor.

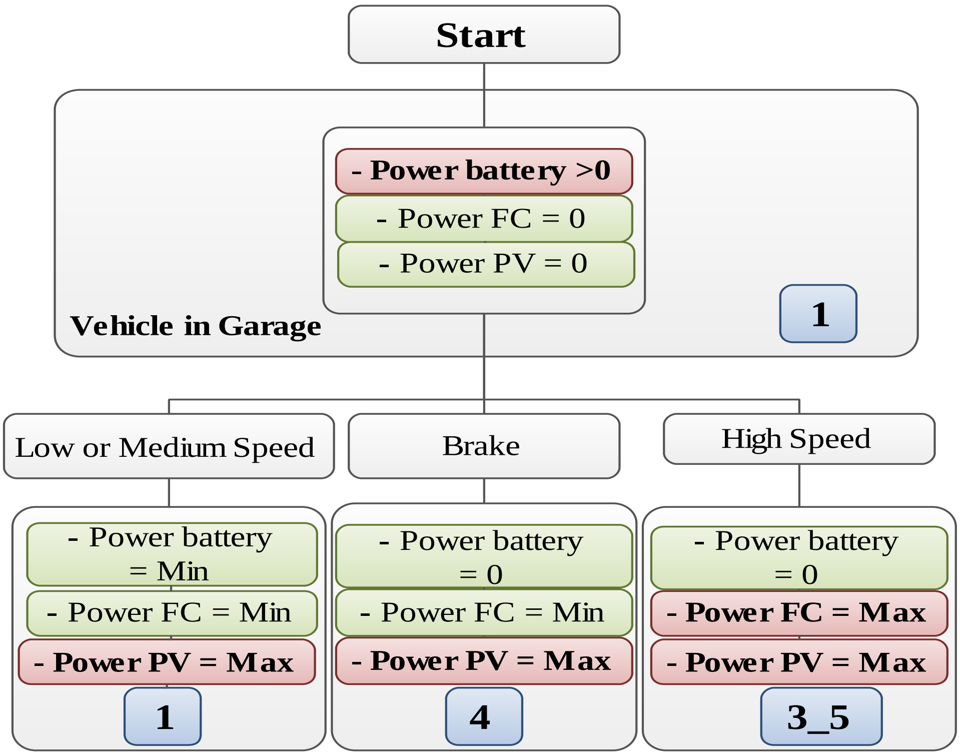

Figure 8. Energy management strategy technique.

Similarly, the fuel cell power evolution can be found in Figure 9b. It is clear that, even if the acceleration factor rises, the fuel cell generates more power. In Figure 9d, the motor's power evolution is proportional to the acceleration factor, which explains why the motor's power increases in the highest acceleration region. Based on Figure 9c, the power needed from the battery system was evaluated. The battery will contribute significantly only if the PV system is used as it is in the period with a 0.5 acceleration ratio. However, if the fuel cell is integrated in addition to the PV system, the given battery power will be less, and it will be less than 10 KW before the new acceleration ratio is given. Therefore, it is clear that the battery can provide a maximum given power, reaching 42 KW in the traction mode. However, in the recharging mode, as it is during deceleration, when the acceleration ratio is 0, the injected power inside the battery reaches 38 KW at the beginning of this deceleration mode.

It is essential to mention that the battery specification used in this simulation phase is as mentioned in Table 3. A value of 50 kW is the rated battery power.

In addition, one of the simulation conditions is related to the non-activation of the regenerative mode. Similarly, the PV will contribute 100% of its energy in the recharging phase and cover the shortfall through the use of the FC system. Thus, the battery power will be harmful as it receives energy from the recharging tool, as shown in Figure 9c.

5.3. Efficiency of a Hybrid System: Dynamic Mode and Static Mode

In this section, it is supposed that the vehicle comportment was simulated for 15 s. However, for the hybrid proficiency test, it is mandatory to know the SOC status of the battery for the different vehicle conditions. So, two cases were investigated. The first case examined the dynamic mode where the vehicle is in motion with variable speed. The second case is the static mode, which studied the stopped car situation and shows the recharging system performance. In both cases, the effect of the hybrid system on the SOC of the battery was observed.

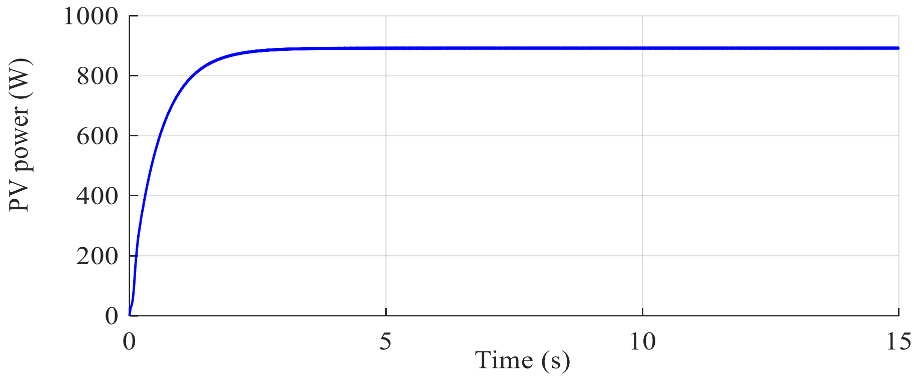

(**a**)

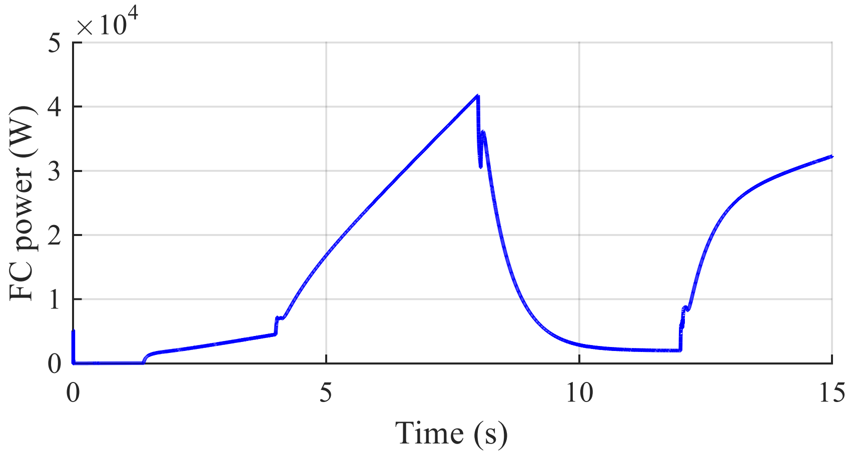

(**b**)

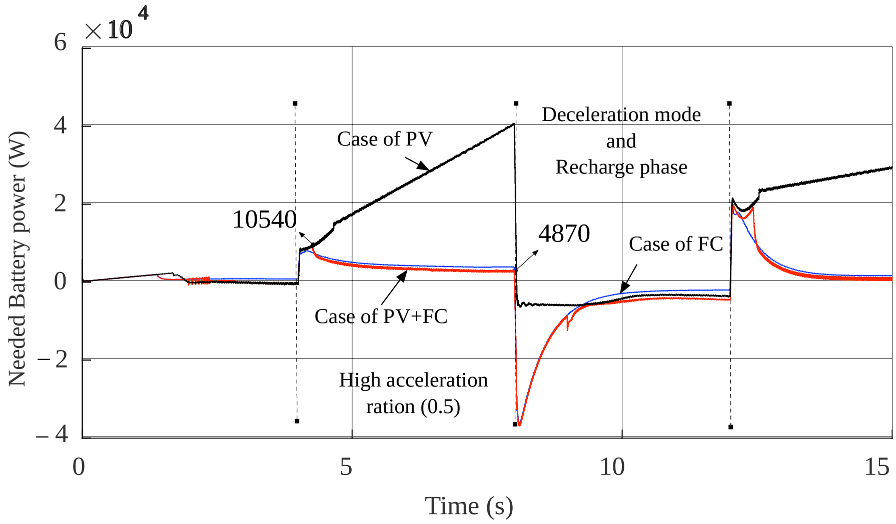

(**c**)

Figure 9. *Cont.*

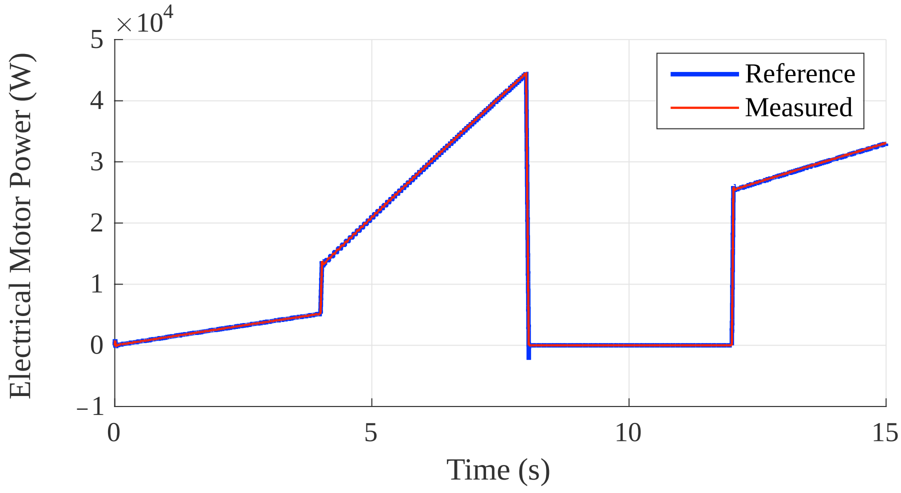

(**d**)

Figure 9. (**a**) Photovoltaic generator power; (**b**) fuel cell power; (**c**) battery power; (**d**) power delivered to the electric motor by the three sources.

5.3.1. Case 1: Dynamic Mode

In this case, the electric vehicle was driven using the electric motor. The primary energy management strategy in combined systems is stated in many works. Figure 10 shows the state of charge of the lithium-ion battery. From the obtained results, the hybrid system can control all energy loops efficiently, as specified by the control of energy management in Figure 8. The sudden changes in rotating speed at t = 4 s, t = 8 s, and t = 12 s were made to check the hybrid system's robustness. The outcomes of the model validate the proposed hypothesis.

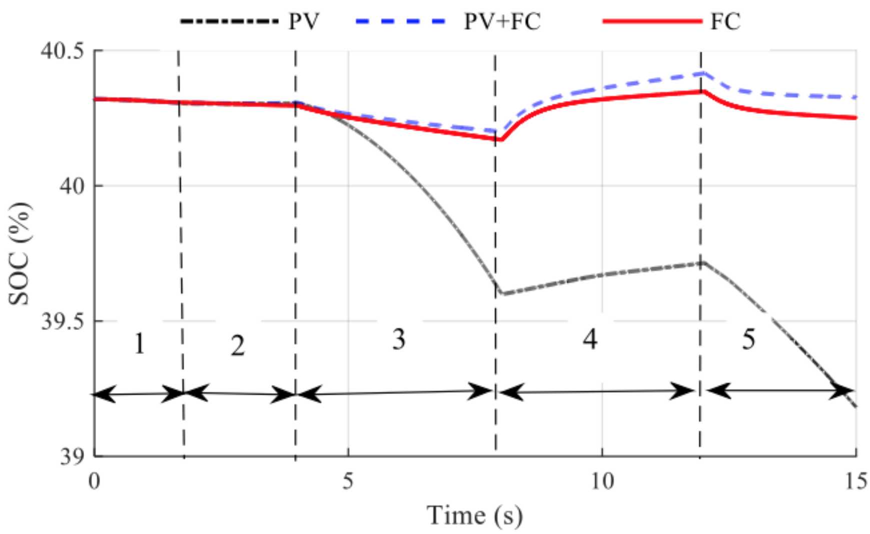

Figure 10. Battery state of charge with the charger system.

5.3.2. Case 2: Static Mode

In this case, it was assumed that the electric motor was inactive and the battery was only being charged. Figure 11 shows the results of the battery SOC for the different charging systems. In this simulation, the initial value of the SOC was equal to 40.32%, and the energy gain from each recharging system could be estimated. For the case of the PV system, the energy gain was 0.48%, as the new battery SOC was 40.80%. For the FC, the final SOC reached 41.50%, and then the gain was 1.18%. For the combined source (PV + FV), the obtained SOC was 42.90%, and the gain was 2.58%. Therefore, it can be concluded that the FC + PV system is more efficient in energy production.

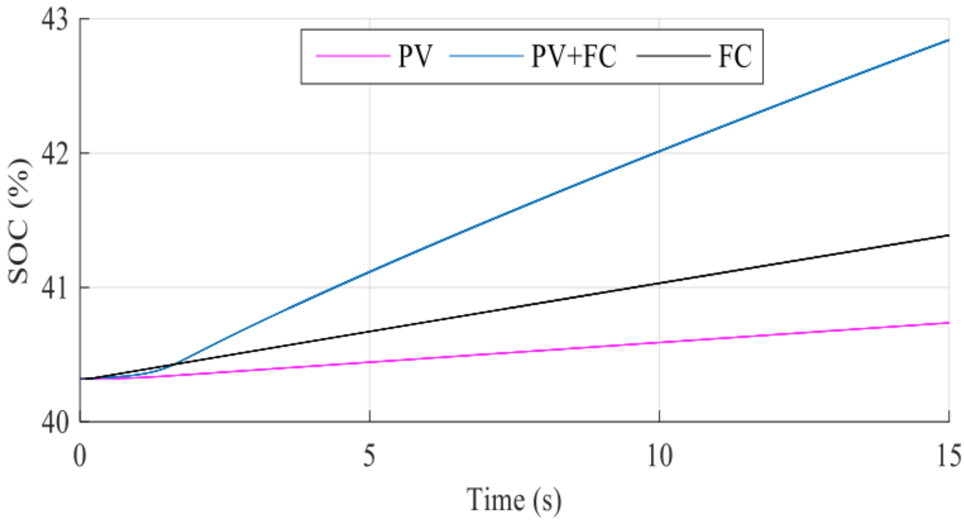

Figure 11. SOC evolution in relation to the different recharging systems.

5.4. Energetic Performance concerning Each Recharging Method

For the same previous simulation conditions, this section will show the energetic performance of the hybrid system. The given evaluation was made under the previous vehicle speeds. According to Figure 10, it was noticed that the zone (zone 4) at t = 8 s and t = 12 s, a deceleration zone, was fixed, but a regenerative mode was not activated. Therefore, the energy gain can be evaluated by presenting the percentage gain for each system. Table 4 shows some statistics and gives an energetic evaluation.

Table 4. Estimated energy gain for each system in the deceleration zone (zone 4).

	Energy Gain		
	PV	**FC**	**PV + FC**
At the beginning of the zone	39.6%	40.17%	40.2%
At the end of the zone	39.71%	40.35%	40.42%
SOC gain	0.11%	0.18%	0.22%

Referring to this case (case 1 and case 2), each recharging technique was tested separately, and their performance and energetic contribution were evaluated in detail. The optimum selection can be related to combining the two techniques (FC and PV), as demonstrated by the given statistics in the case studies. Nevertheless, as the difference is insufficient, the major energy efficiency can only be assessed if the PV system's weight is correctly considered. Based on some research, the evaluation of the influence of the PV system weight on the vehicle was made, and a comparison regarding its influence is summarised in Table 5. It is shown that with the new PV system technique [56,57], the PV systems add more weight to the vehicle, which will slightly affect its performance.

Table 5. Influence of the PV cell weight on the energetic consumption over 100 Km.

	With the Weight of PV	Without the Weight of PV
Example of vehicle model weight	750 kg	737 kg
Energy consumed over 100 km	14.08 kWh	14 kWh

Consequently, it is possible to say that the benefit of this renewable energy source is assured. Nevertheless, it is vital to demonstrate that the vehicle speed factor has a significant influence on the energetic performance, as is demonstrated in [57–59] and as is shown in Figure 12, which shows that in a deceleration mode, the PV cells will contribute 100% to the recharging action. Therefore, the percentage in this figure presents the rate of use of each charging system for each speed. For example, in Figure 12d, for no acceleration action (acceleration = 0), the PV cells contributed 100% to the recharging action. Based on this paper, the proposed solution would help reduce fuel consumption and help charge electric vehicles efficiently. Table 6 shows the benchmarks for many segmented FC and PV system research projects and the results presented in the literature. Compared to [6,9,55,60], the proposed hybrid system uses refined active recharging to produce a high power level of 4900 watts.

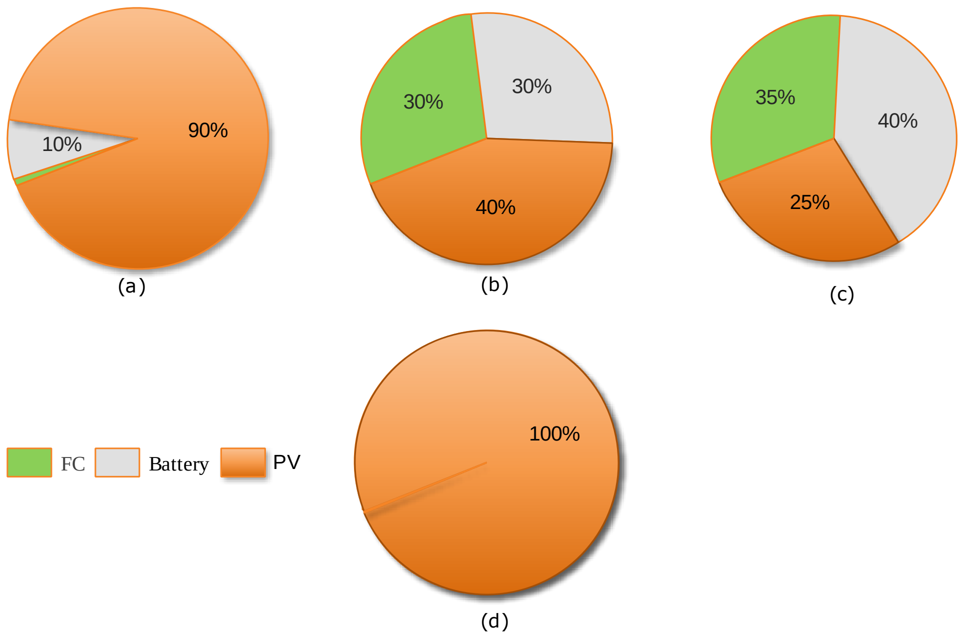

Figure 12. Energetic contribution of the three power generation modes according to the vehicle speed: (**a**) low speed, (**b**) medium speed, (**c**) high speed, and (**d**) no acceleration action.

Table 6. Comparison of different hybrid systems.

References/Parameters	Battery Power (W)	Number of Sources
Proposed system	4900	3
System 1 [9]	5200	4
System 2 [55]	1440	3
System 3 [6]	4986	3
System 4 [60]	3200	2

In Table 6, a comparison between the contribution of the battery pack for more than hybrid energy management tool is compared. Initially, it is important to mention that the battery pack will always be required to help feed the electrical motor with the necessary energy power. As shown in Figure 9c, in the high acceleration period, the battery contributed 10,540 W at the beginning of the acceleration phase and 4870 W at the end of the acceleration mode. Therefore, after this test, it was concluded that the battery pack contributed at least 4900 W, as mentioned in Table 6.

6. Conclusions

This study presents a hybrid recharging tool used for electric vehicles. A complete mathematical model describing the components used and the approach adopted to recharge the battery and provide energy to the traction motor is presented. In this paper, the FC, the PV, or a combination of both was used in the recharging mode. This is why we talk about the hybrid recharging system. The battery pack only feeds the traction mode, and when it is required, the battery is charged through these blocks. The simulated case studies suggest that additive autonomy can be obtained using this hybrid energy combination for recharging and driving. The results signify hybridisation's importance and demonstrate the potential of hybridisation with renewable energy sources in future hybrid electric vehicles. Particularly with PV hybridisation, a significant charging gain while stationary without the need to plug the car into a socket can be useful for regions with higher solar irradiance. A comparison with previous studies suggests that the proposed recharging model is significantly effective. The study can be used as a steppingstone to develop further detailed studies by considering additional variables, such as the cost of the components, the vehicle weight, the regenerative system, and many others.

Author Contributions: S.L., F.A. and N.M. designed the problem under study, performed the simulations, and obtained the results; A.A., Z.A.K. and S.L. analysed the obtained results; F.A., Z.A.K., A.A. and N.M. wrote the paper, which was further reviewed by all authors. All authors have read and agreed to the published version of the manuscript.

Funding: This research was funded by Majmaah University, grant number R-2021-229.

Institutional Review Board Statement: Not applicable.

Informed Consent Statement: Not applicable.

Data Availability Statement: Data sharing is not applicable to this article.

Acknowledgments: The authors would like to thank the Deanship of Scientific Research at Majmaah University for supporting this work under project number R-2021-229.

Conflicts of Interest: The authors declare no conflict of interest.

Abbreviations

EV	Electric Vehicle
FC	Fuel Cell
IPT	Inductive Power Transfer
PV	Photovoltaic
HEV	Hybrid Electric Vehicles
BEV	Battery Electric Vehicles
ICE	Internal Combustion Engine
GV	Gasoline Vehicle
FCV	Fuel Cell Vehicle
SOC	State of Charge
List of symbols	
$E_{on,IGBT}$	IGBT ON state (J)
$E_{off,IGBT}$	IGBT OFF state (J)
$E_{on,M}$	MOSFET on state energy loss (J)
$E_{off,M}$	MOSFET off-state energy loss (J)
ESR	Effective series resistance (Ω)
f_{sw}	Switching frequency (kHz)
i_C	Collector current (A)
I_{Cav}	Average collector current (A)
I_{Crms}	Collector RMS current (A)
i_D	Drain current (A)
i_{Drms}	Drain RMS current (A)
I_{Lrms}	Inductor RMS current (A)
I_0	Output current (A)
V_{fD}	Diode on-state voltage drop (V)
V_0	Output DC voltage (V)

$P_{con,\,D}$	Diode conduction loss (W)
$P_{con,M}$	MOSFET conduction loss (W)
$P_{con,IGBT}$	IGBT conduction loss (W)
$P_{sw,IGBT}$	IGBT switching loss (W)
$P_{sw,M}$	MOSFET switching loss (W)
Q_c	Schottky diode junction charge (C)
R_C	Collector resistance (Ω)
R_{dc}	Inductor DC resistance (Ω)
$R_{DS(on)}$	Drain to source on resistance (Ω)
T_{sw}	Switching period (s)
v_{CE}	Instantaneous collector to emitter voltage (V)
v_{CEO}	Collector voltage (V)
v_{DS}	Instantaneous drain to source voltage (V)
V_{DS}	Off condition of the drain to source voltage in (V)
T	Cell temperature in Kelvin (K)
q	Electron charge (1.602×10^{-19} C)
K	Boltzmann's constant (1.381×10^{-23} J/K)
I_{rs}	Saturation current of the diode
P_{fuel}	Pressure of fuel (atm)
P_{air}	Pressure of air (atm)
$V_{lpm(fuel)}$	Fuel flow rate (l min^{-1})
$V_{lpm(air)}$	Airflow rate (l min^{-1})
x	Hydrogen in the fuel (%)
y	Oxygen in the oxidant (%)
N	Cell number
z	Moving electrons
Kc	Voltage of nominal operation conditions (V)
k	Boltzmann's constant [J K^{-1}]
h	Planck constant [J s]
η_{nom}	Nominal efficiency (%)
$\Delta h^0_{(H_2O)g}$	Enthalpy of water vapour (J mol^{-1})
V_{nom}	Nominal voltage (V)
I_{nom}	Nominal current (A)
i_{fc}	FC current (A)
$V_{Ipm(air)nom}$	Nominal airflow rate (l min^{-1})
A	Exponential zone amplitude (V)
P_{airnom}	Nominal absolute pressure of air (Pa)
Q	Battery capacity (Ah)
T_{nom}	Nominal operating temperature (K)
I^*	Current of low-frequency dynamic (A)
P_{H_2O}	Water pressure (bar)
it	Available capacity (Ah)
ω	Percentage in the oxidant (%)
K	Polarisation constant or polarisation resistance (Ω)
B	Exponential zone time constant inverse $(\text{Ah})^{-1}$
E_0	Standard voltage (V)
E_{batt}	Nonlinear voltage (V)

References

1. Alam Chowdhury, M.S.; Rahman, A.M.; Samrat, N.H. A comprehensive study on green technologies used in the vehicle. In Proceedings of the 2015 3rd International Conference on Green Energy and Technology (ICGET), Dhaka, Bangladesh, 11 September 2015.
2. Ahmad, S.; Ahmad, A.; Naeem, M.; Ejaz, W.; Kim, H.S. A compendium of performance metrics, pricing schemes, optimisation objectives, and solution methodologies of demand side management for the smart grid. *Energies* **2018**, *11*, 2801. [CrossRef]
3. Thomas, C.E. Fuel cell and battery electric vehicles compared. *Int. J. Hydrogen Energy* **2009**, *34*, 6005–6020. [CrossRef]
4. Hwang, J.J.; Wang, D.Y.; Shih, N.C. Development of a lightweight fuel cell vehicle. *J. Power Sources* **2005**, *141*, 108–115. [CrossRef]
5. Veziroglu, A.; MacArio, R. Fuel cell vehicles: State of the art with economic and environmental concerns. *Int. J. Hydrogen Energy* **2011**, *36*, 25–43. [CrossRef]

6. Mohamed, N.; Aymen, F.; Ali, Z.M.; Zobaa, A.F.; Aleem, S.H.E.A. Efficient Power Management Strategy of Electric Vehicles Based Hybrid Renewable Energy. *Sustainability* **2021**, *13*, 7351. [CrossRef]
7. Zhang, R.; Tao, J.; Zhou, H. Fuzzy Optimal Energy Management for Fuel Cell and Supercapacitor Systems Using Neural Network Based Driving Pattern Recognition. *IEEE Trans. Fuzzy Syst.* **2019**, *27*, 45–57. [CrossRef]
8. Moore, R.M.; Hauer, K.H.; Friedman, D.; Cunningham, J.; Badrinarayanan, P.; Ramaswamy, S.; Eggert, A. A dynamic simulation tool for hydrogen fuel cell vehicles. *J. Power Sources* **2005**, *141*, 272–285. [CrossRef]
9. Mokrani, Z.; Rekioua, D.; Rekioua, T. Modeling, control and power management of hybrid photovoltaic fuel cells with battery bank supplying electric vehicle. *Int. J. Hydrogen Energy* **2014**, *39*, 15178–15187. [CrossRef]
10. Hwang, J.J.; Chen, Y.J.; Kuo, J.K. The study on the power management system in a fuel cell hybrid vehicle. *Int. J. Hydrogen Energy* **2012**, *37*, 4476–4489. [CrossRef]
11. Wang, M. Fuel choices for fuel-cell vehicles: Well-to-wheels energy and emission impacts. *J. Power Sources* **2002**, *112*, 307–321. [CrossRef]
12. Hwang, J.J.; Kuo, J.K.; Wu, W.; Chang, W.R.; Lin, C.H.; Wang, S.E. Lifecycle performance assessment of fuel cell/battery electric vehicles. *Int. J. Hydrogen Energy* **2013**, *38*, 3433–3446. [CrossRef]
13. Un-Noor, F.; Padmanaban, S.; Mihet-Popa, L.; Mollah, M.N.; Hossain, E. A comprehensive study of key electric vehicle (EV) components, technologies, challenges, impacts, and future direction of development. *Energies* **2017**, *10*, 1217. [CrossRef]
14. Boretti, A. Analysis of the energy storage battery and fuel tank of a commercial electric vehicle with range extender during charge sustaining operation. *Energy Storage* **2020**, *2*, e129. [CrossRef]
15. Baek, K.; Kim, S.; Lee, E.; Cho, Y.; Kim, J. Data-Driven Evaluation for Demand Flexibility of Segmented Electric Vehicle Chargers in the Korean Residential Sector. *Energies* **2021**, *14*, 866. [CrossRef]
16. Ahmad, S.; Alhaisoni, M.M.; Naeem, M.; Ahmad, A.; Altaf, M. Joint Energy Management and Energy Trading in Residential Microgrid System. *IEEE Access* **2020**, *8*, 123334–123346. [CrossRef]
17. Lulhe, A.M.; Date, T.N. A technology review paper for drives used in electrical vehicle (EV) & hybrid electrical vehicles (HEV). In Proceedings of the 2015 International Conference on Control, Instrumentation, Communication and Computational Technologies ICCICCT, Kumaracoil, India, 18–19 December 2015; pp. 632–636.
18. Mohamed, N.; Aymen, F.; Alqarni, M. Inductive Power Transmission System for Electric Car Charging Phase: Modeling plus Frequency Analysis. *World Electr. Veh. J.* **2021**, *12*, 267. [CrossRef]
19. Datta, U. A price-regulated electric vehicle charge-discharge strategy. *Energy Res.* **2019**, *43*, 1032–1042. [CrossRef]
20. Rawat, T.; Niazi, K.R.; Gupta, N.; Sharma, S. Impact assessment of electric vehicle charging/discharging strategies on the operation management of grid accessible and remote microgrids. *Int. J. Energy Res.* **2019**, *43*, 9034–9048. [CrossRef]
21. Models, T.; Kim, Y.; Kim, S. Forecasting Charging Demand of Electric Vehicles Using Time-Series Models. *Energies* **2021**, *14*, 1487.
22. Mohamed, N.; Aymen, F.; Issam, Z.; Bajaj, M.; Ghoneim, S.S.M. The Impact of Coil Position and Number on Wireless System Performance for Electric Vehicle Recharging. *Sensors* **2021**, *21*, 4343. [CrossRef]
23. Song, Z.; Hofmann, H.; Li, J.; Wang, Y.; Lu, D.; Ouyang, M.; Du, J. Torque Distribution Strategy for Multi-PMSM Applications and Optimal Acceleration Control for Four-Wheel-Drive Electric Vehicles. *J. Dyn. Syst. Meas. Control* **2019**, *142*, 021001. [CrossRef]
24. Habib, S.; Khan, M.M.; Abbas, F.; Ali, A.; Faiz, M.T.; Ehsan, F.; Tang, H. Contemporary trends in power electronics converters for charging solutions of electric vehicles. *CSEE J. Power Energy Syst.* **2020**, *6*, 911–929.
25. Tie, S.S.F.; Tan, C.W.C. A review of energy sources and energy management system in electric vehicles. *Renew. Sustain. Energy Rev.* **2013**, *20*, 82–102. [CrossRef]
26. Tan, K.M.; Ramachandaramurthy, V.K.; Yong, J.Y. Integration of electric vehicles in smart grid: A review on vehicle to grid technologies and optimisation techniques. *Renew. Sustain. Energy Rev.* **2016**, *53*, 720–732. [CrossRef]
27. Lipu, M.S.H.; Faisal, M.; Ansari, S.; Hannan, M.A.; Karim, T.F.; Ayob, A.; Hussain, A.; Miah, M.S.; Saad, M.H.M. Review of Electric Vehicle Converter Configurations, Control Schemes and Optimizations: Challenges and Suggestions. *Electronics* **2021**, *10*, 477. [CrossRef]
28. Naoui, M.; Aymen, F.; Ben Hamed, M.; Lassaad, S. Analysis of Battery-EV state of charge for a Dynamic Wireless Charging system. *Energy Storage* **2019**, *2*, e117.
29. Zhuang, Z.; Yang, L.; Ju, B.; Yin, A.; Lei, G.; Zhou, Q.; Tang, Y.; Deng, Z.; Tu, F.; Qin, S. Engineering $LiNi_{0.5}Co_{0.2}Mn_{0.3}O_2$/poly-(propylene carbonate) interface by graphene oxide modification for all-solid-state lithium batteries. *Energy Storage* **2020**, *2*, e109. [CrossRef]
30. Lee, J.Y.; Han, B.M. A bidirectional wireless power transfer EV charger using self-resonant PWM. *IEEE Trans. Power Electron.* **2015**, *30*, 1784–1787. [CrossRef]
31. Tremblay, O.; Dessaint, L. Experimental Validation of a Battery Dynamic Model for EV Applications. *World Electr. Veh. J.* **2009**, *3*, 289–298. [CrossRef]
32. Dubarry, M.; Vuillaume, N.; Liaw, B.Y. From single cell model to battery pack simulation for Li-ion batteries. *J. Power Sources* **2009**, *186*, 500–507. [CrossRef]
33. Rothenberger, M.J.; Safi, J.; Liu, J.; Anstrom, J.; Brennan, S.; Fathy, H.K. Improving Lithium-Ion Battery Pack Diagnostics by Optimising the Internal Allocation of Demand Current for Parameter Identifiability. *J. Dyn. Syst. Meas. Control* **2017**, *139*, 081001. [CrossRef]

34. Mohamed, N.; Aymen, F.; Lassaad, S.; Mouna, B.H. Practical validation of the vehicle speed influence on the wireless recharge system efficiency. In Proceedings of the 2020 6th IEEE International Energy Conference (ENERGYCon), Gammarth, Tunisia, 28 September–1 October 2020; pp. 372–376.
35. Dhameja, S. Electric Vehicle Battery Charging. In *Electric Vehicle Battery Systems*; Butterworth–Heinemann: Woburn, MA, USA, 2001; pp. 69–91.
36. Baliga, B.J. Power Semiconductor Device Figure of Merit for High-Frequency Applications. *IEEE Electron Device Lett.* **1989**, *10*, 455–457. [CrossRef]
37. Elasser, A.; Chow, T.P. Silicon carbide benefits and advantages for power electronics circuits and systems. *Proc. IEEE* **2002**, *90*, 969–986. [CrossRef]
38. Hudgins, J.L.; Simin, G.S.; Santi, E.; Khan, M.A. An assessment of wide band-gap semiconductors for power devices. *IEEE Trans. Power Electron.* **2003**, *18*, 907–914. [CrossRef]
39. El Fadil, H.; Giri, F.; Member, S.; Guerrero, J.M.; Member, S. Modeling and Nonlinear Control of a Fuel Cell/Supercapacitor Hybrid Energy Storage System for Electric Vehicles. *IEEE Trans. Veh. Technol.* **2014**, *63*, 3011–3018. [CrossRef]
40. Alam, M.; Kumar, K.; Dutta, V. Comparative efficiency analysis for silicon, silicon carbide MOSFETs and IGBT device for DC–DC boost converter. *SN Appl. Sci.* **2019**, *1*, 1–11. [CrossRef]
41. Mohamed, N.; Aymen, F.; Hamed, M. Ben Characteristic Of Photovoltaic Generator For The Electric Vehicle. *Int. J. Sci. Technol. Res.* **2019**, *8*, 871–876.
42. Ahmed, M.; Abdelrahem, M.; Harbi, I.; Kennel, R. An Adaptive Model-Based MPPT Technique with Drift-Avoidance for Grid-Connected PV Systems. *Energies* **2020**, *13*, 6656. [CrossRef]
43. Bendjedia, B.; Hadjadj, A.; Benhouia, A.; Temmir, T. Energy management and control of a solar electric vehicle. In Proceedings of the 2015 4th International Conference on Electrical Engineering (ICEE), Boumerdes, Algeria, 13–15 December 2015; pp. 1–5. [CrossRef]
44. Ye, B.; Jiang, J.; Miao, L.; Yang, P.; Li, J.; Shen, B.; Ye, B.; Jiang, J.; Miao, L.; Yang, P.; et al. Feasibility Study of a Solar-Powered Electric Vehicle Charging Station Model. *Energies* **2015**, *8*, 13265–13283. [CrossRef]
45. Paladini, V.; Donateo, T.; de Risi, A.; Laforgia, D. Super-capacitors fuel-cell hybrid electric vehicle optimisation and control strategy development. *Energy Convers. Manag.* **2007**, *48*, 3001–3008. [CrossRef]
46. Cipollone, R.; Di Battista, D.; Marchionni, M.; Villante, C. Model based design and optimisation of a fuel cell electric vehicle. *Energy Procedia* **2014**, *45*, 71–80. [CrossRef]
47. Hwang, J.J.; Chen, C.K.; Savinell, R.F.; Liu, C.C.; Wainright, J. A three-dimensional numerical simulation of the transport phenomena in the cathodic side of a PEMFC. *J. Appl. Electrochem.* **2004**, *34*, 217–224. [CrossRef]
48. Andaloro, L.; Arista, A.; Agnello, G.; Napoli, G.; Sergi, F.; Antonucci, V. Study and design of a hybrid electric vehicle (Lithium Batteries-PEM FC). *Int. J. Hydrogen Energy* **2017**, *42*, 3166–3184. [CrossRef]
49. Schouten, N.J.; Salman, M.A.; Kheir, N.A. Fuzzy logic control for parallel hybrid vehicles. *IEEE Trans. Control Syst. Technol.* **2002**, *10*, 460–468. [CrossRef]
50. Fu, Z.; Zhu, L.; Tao, F.; Si, P.; Sun, L. Optimization based energy management strategy for fuel cell/battery/ultracapacitor hybrid vehicle considering fuel economy and fuel cell lifespan. *Int. J. Hydrogen Energy* **2020**, *45*, 8875–8886. [CrossRef]
51. Hoenicke, P.; Ghosh, D.; Muhandes, A.; Bhattacharya, S.; Bauer, C.; Kallo, J.; Willich, C. Power management control and delivery module for a hybrid electric aircraft using fuel cell and battery. *Energy Convers. Manag.* **2021**, *244*, 114445. [CrossRef]
52. Tran, D.D.; Vafaeipour, M.; El Baghdadi, M.; Barrero, R.; Van Mierlo, J.; Hegazy, O. Thorough state-of-the-art analysis of electric and hybrid vehicle powertrains: Topologies and integrated energy management strategies. *Renew. Sustain. Energy Rev.* **2020**, *119*, 109596. [CrossRef]
53. Ahmad, S.; Naeem, M.; Ahmad, A. Unified optimisation model for energy management in sustainable smart power systems. *Int. Trans. Electr. Energy Syst.* **2020**, *30*, e12144. [CrossRef]
54. Nguyen, B.H.; Trovão, J.P.F.; German, R.; Bouscayrol, A. Real-time energy management of parallel hybrid electric vehicles using linear quadratic regulation. *Energies* **2020**, *13*, 5538. [CrossRef]
55. Zhang, Y.; Ma, R.; Zhao, D.; Huangfu, Y.; Liu, W. A Novel Energy Management Strategy based on Dual Reward Function Q-learning for Fuel Cell Hybrid Electric Vehicle. *IEEE Trans. Ind. Electron.* **2021**, *69*, 1537–1547. [CrossRef]
56. Oberbeck, L.; Alvino, K.; Goraya, B.; Jubault, M. IPVF's PV technology vision for 2030. *Prog. Photovolt. Res. Appl.* **2020**, *28*, 1207–1214. [CrossRef]
57. Sierra, A.; Reinders, A. Designing innovative solutions for solar-powered electric mobility applications. *Prog. Photovolt. Res. Appl.* **2020**, *29*, 802–818. [CrossRef]
58. Das, H.S.; Rahman, M.M.; Li, S.; Tan, C.W. Electric vehicles standards, charging infrastructure, and impact on grid integration: A technological review. *Renew. Sustain. Energy Rev.* **2020**, *120*, 109618. [CrossRef]
59. Turoń, K. Hydrogen-powered vehicles in urban transport systems-current state and development. *Transp. Res. Procedia* **2020**, *45*, 835–841. [CrossRef]
60. Okundamiya, M.S. Size optimisation of a hybrid photovoltaic/fuel cell grid connected power system including hydrogen storage. *Int. J. Hydrogen Energy* **2021**, *46*, 30539–30546. [CrossRef]